

# Search for multiwavelength emission from the binary millisecond pulsar PSR J1836-2354A in the globular cluster M22

R. Amato<sup>1,2,3</sup>, A. D’Ai<sup>2</sup>, M. Del Santo<sup>2</sup>, D. de Martino<sup>4</sup>, A. Marino<sup>1,2,5</sup>, T. Di Salvo<sup>1</sup>, R. Iaria<sup>1</sup>, T. Mineo<sup>2</sup>

<sup>1</sup> *Università degli Studi di Palermo, Dipartimento di Fisica e Chimica, via Archirafi 36, I-90123 Palermo, Italy*

<sup>2</sup> *INAF - IASF Palermo, Via U. La Malfa 153, I-90146 Palermo, Italy*

<sup>3</sup> *IAAT Universität Tübingen, Sand 1, D-72076 Tübingen, Germany*

<sup>4</sup> *INAF - Osservatorio Astronomico di Capodimonte, Salita Moiariello 16, I-80131 Napoli, Italy*

<sup>5</sup> *IRAP, Université de Toulouse, CNRS, UPS, CNES, Toulouse, France.*

17 April 2019

## ABSTRACT

We present a multi-band search for X-ray, optical and  $\gamma$ -ray emission of the radio binary millisecond pulsar J1836-2354A, hosted in the globular cluster M22. X-ray emission is significantly detected in two *Chandra* observations, performed in 2005 and 2014, at a luminosity of  $\sim 2\text{--}3 \times 10^{30}$  erg s<sup>-1</sup>, in the 0.5–8 keV energy range. The radio and the X-ray source positions are found consistent within  $1\sigma$  error box. No detection is found in archival *XMM-Newton* and *Swift*/XRT observations, compatible with the *Chandra* flux level. The low statistics prevents us to assess if the X-ray source varied between the two observations. The X-ray spectrum is consistent with a power-law of photon index  $\sim 1.5$ . We favour as the most probable origin of the X-ray emission an intrabinary shock scenario. We searched for optical and  $\gamma$ -ray counterparts to the radio source using data from *Hubble Space Telescope* and *Fermi*-LAT catalogues, respectively. No optical counterpart down to  $V=25.9$  and  $I=24.7$  ( $3\sigma$ ) is detected, which suggests a companion mass of 0.1–0.2  $M_{\odot}$ . Combined with the low X-ray luminosity, this is consistent with a black widow nature of PSR J1836-2354A. Inspecting the 8-year *Fermi*-LAT catalogue, we found a  $\gamma$ -ray source, 4FGL J1836.8–2354, with a positional uncertainty consistent with the globular cluster, but not with the radio position of the millisecond pulsar.

**Key words:** X-rays: binaries – X-rays: individual: PSR J1836-2354A – Stars: pulsars – Galaxy: globular clusters: individual: M22 (NGC 6656).

## 1 INTRODUCTION

Millisecond pulsars (MSPs) are neutron stars (NSs) emitting radio pulsed radiation at their spin periods. They can be isolated or in binary systems. According to the recycling scenario (Alpar et al. 1982), MSPs are the outcome of accretion onto the NS of mass transferred from a late-type companion. After Gyr-long mass accretion phase during which these systems appear as low-mass X-ray binaries (LMXBs), the mass transfer rate declines allowing the activation of a radio and/or  $\gamma$ -ray pulsar powered by rotation of its magnetic field (Bhattacharya & van den Heuvel 1991, Burderi et al. 2001). A few systems - three so far - were found to transit from an accretion to a rotation-powered state and viceversa proving the existence of the link between LMXBs and MSPs (Papitto et al. 2013, Bassa et al. 2014, Stappers et al. 2014).

Globular clusters (GCs) are the densest environments in our Galaxy where MSPs can be found. Their high stellar densities imply a high rate of dynamical interactions, such that binary systems are

formed through alternative mechanisms to the normal evolutionary channels, e.g. tidal capture (Fabian et al. 1975), collisions with a giant star (Sutantyo 1975) or by exchange between primordial binaries (Hills 1976). Moreover, due to the aged population, binary systems in GCs are predominantly constituted of a compact object, like white dwarfs (WDs) or NSs, which accretes matter from its companion, usually a low-mass Main Sequence star. Hence, the X-ray population in GCs is mainly constituted by a mixture of quiescent LMXBs, Cataclysmic Variables (CVs), MSPs and Chromospherical Active Binaries (ABs) (see Heinke 2010, for a review).

M22 (NGC 6656) is one of the most luminous GC in the Milky Way. At a distance of 3.2 kpc, it has a projected core radius ( $r_{core}$ ) of 1.33' and a half-mass radius of 3.36' (Harris 1996, 2010 edition), a tidal radius of 31.9' (Alonso-García et al. 2012), a total mass of  $\sim 5 \times 10^5 M_{\odot}$  (Cheng et al. 2018) and an absolute age of 12.67 Gyr (Forbes & Bridges 2010). Lynch et al. (2011) reported the detection of two radio MSPs in this GC: J1836-2354A and J1836-2354B. J1836-2354A (M22A, hereafter) is a 3.35 ms pulsar

in a binary system with an orbital period of 4.87 h, negligible eccentricity,  $a \sin(i) = 0.046412$  lt-s, a mass function of  $2.609(1) \times 10^{-6}$  and a minimum mass of  $0.017 M_{\odot}$  for the companion star. An extremely low mass secondary would indicate M22A as a black widow system, rather than a redback system, which instead harbours a non-degenerate secondary (i.e.  $M_2 \geq 0.1 M_{\odot}$ ) (Roberts et al. 2018). The other pulsar (M22B hereafter) is isolated with a 3.23 ms spin period. Both pulsars lie within the cluster core radius.

Besides the radio emission, MSPs can also be detected in other bands, thus allowing to probe different environments and processes in, or close to, the pulsar magnetosphere, e.g. optical emission can come from the companion star or, in the case of a LMXBs, from the accretion disk (Archibald et al. 2009), when present.

Furthermore,  $\gamma$ -ray emission from Galactic GCs has been detected by the LAT instrument on board of *Fermi Gamma Ray Space Telescope* (*Fermi-LAT*, hereafter) since its launch, in 2008. Being MSPs strong emitters of  $\gamma$ -rays (Chen 1991, Harding et al. 2005) and being GCs extremely rich of MSPs, the whole  $\gamma$ -ray emission from GCs is thought to be the convolution of the emission from all the MSPs in a cluster (Abdo et al. 2010, Caraveo 2014).  $\gamma$ -ray emission from M22 was only recently detected by *Fermi-LAT* (Zhou et al. 2015), after more than 6 years of observations. A flux of  $(8.6 \pm 1.9) \times 10^{-12}$  erg cm $^{-2}$  s $^{-1}$  was derived by fitting the spectrum with a power law model with a spectral index of  $2.7 \pm 0.1$ , in the energy range 0.1-100 GeV.

The first X-ray observations of M22 were made with *Einstein* (Hertz & Grindlay 1983) and *ROSAT* (Johnston et al. 1994). More recently, *XMM-Newton* observed the cluster in 2000 (Webb et al. 2002, 2004) while *Chandra* in 2005 (Webb & Servillat 2013) and in 2014. Webb & Servillat (2013) analysed the *Chandra* observation made in 2005 and reported a faint X-ray source (Source 3 in their Table 1) as the possible X-ray counterpart of M22A. We use all the available archival data from *Chandra* and *XMM-Newton*, focusing especially on the longest *Chandra* observation (2014). We also analysed 28 observations performed with the *X-ray Telescope* (XRT, Burrows et al. 2005) instrument on board of the *Neil Gehrels Swift Observatory* (Gehrels et al. 2004, *Swift* hereafter), which has been monitoring the cluster for the past two years. We also performed a search for the optical counterpart using the *Hubble Space Telescope* (*HST*) catalogue from the HUGS project (Piotto et al. 2015), as well as we inspected the 4-year *Fermi-LAT* catalogue (3FGL; Acero et al. (2015) and the 8-yr catalogue (4FGL; The *Fermi-LAT* collaboration (2019)).

## 2 X-RAY OBSERVATIONS AND DATA REDUCTION

We analysed two *Chandra* observations of M22, made on 2005 May 24 for 15.82 ks with ACIS-S in the FAINT mode (Observation ID 5437) and on 2014 May 22 for 84.86 ks with ACIS-S in the VFaint mode (ObsID 14609). For data extraction and analysis we used CIAO version 4.10 and CALDB version 4.7.7. Data sets were reprocessed without including pixel randomization (the parameter PIX\_ADJ was set to EDSEr), in order to slightly improve the point-spread function (PSF).

The *XMM-Newton* observation of M22 was performed on 2000 September 19 (ObsID 0112220201), for a total exposure of 41.2 ks, using the EPIC instruments (pn, MOS1 and MOS2) in imaging mode with the medium filters. We reprocessed the data to obtain calibrated and concatenated event lists with the Science Analysis Software (SAS) version 16.0.0. We produced images for all the EPIC

instruments in three different energy ranges: 0.5-2 keV, 2-4 keV, and 4-10 keV.

We analysed all the *Swift*/XRT observations of the source performed between March 2017 and August 2018. The full XRT observation log consists of 28 pointings of 1–3 ks exposure each, with approximately one or two visits per month. All the data were taken in Photon Counting (PC) mode. Data were reprocessed with XRT-PIPELINE to obtain the cleaned event files and exposure maps, using R.A. and Dec. of the source, as detected in the *Chandra* ObsID 14609 (R.A. = 18:36:25.375, Dec. = -23:54:51.08, in the J2000 system). We merged all the observations, combined the event lists and exposure maps, using the XIMAGE, version 4.5.1 package. Finally, we extracted the image from the merged event list file. The log of all the analysed X-ray observations is reported in Table 1.

## 3 SOURCE DETECTION AND ASTROMETRIC CORRECTIONS OF THE *Chandra* OBSERVATION

The radio position of M22A determined by Lynch et al. (2011) is 2.2' and 0.9' offset from the *Chandra* pointing directions of the 2004 and 2014 observations, respectively. This ensures negligible distortion of the PSF and hence a high accuracy in determining the position of the source. For each observation, we created an exposure-corrected image and exposure map using the FLUXIMAGE tool with a binning equal to 1; we used the tool MKPSFMAP to determine the PSF-size at each pixel. We selected two different energy bands, 0.3–10 keV and 0.5–6 keV, and for these bands we set the encircled counts fraction (ECF) equal to 0.5, while the energy of the PSF was equal to 1.4 keV and 0.3 keV for the broader and for the softer energy band, respectively. We used the source detection tool WAVDETECT with pixel wavelength radii of 1.0, 1.4, 2.0, 2.8, 4.0, 5.6. The probability threshold was left to the default value of  $10^6$  (corresponding to one spurious source in a 1000×1000 pixel map). Image and detection regions (corresponding to a  $3\sigma$  error on the position) are shown in Fig. 1. We limited our analysis to the ACIS-S3 chip.

A X-ray source is found at R.A. = 18:36:25.5(8) and Dec. = -23:54:51.5(5), with  $1\sigma$  errors, in the 2014 observation. The position detected in the 2005 observation differs of 0.1'' in R.A. with respect to the 2014 one. These are consistent with that reported by Webb & Servillat (2013), although with a slightly larger uncertainty, likely due to the different source extraction procedure (ACIS-Extract). The detection is always consistent with a point-like source, with no evidence of extended emission. The X-ray source is found to be at 0.2'' East and 0.9'' North from the radio position of M22A. Since the long 84 ks *Chandra* exposure could be affected by the spacecraft drift, we improved the absolute astrometry, using a cross-matching method.

For this purpose, we used the UV-optical catalogue of M22 from the *HST* UV Globular Cluster Survey (HUGS; Piotto et al. 2015, Nardiello et al. 2018, see Section 5), available at the University of Padua<sup>1</sup>. The catalogue covers an area of about 4'×4', centred on the cluster core. The surveys also encompass two distant regions (parallel fields, Simioni et al. 2018), but none of the X-ray sources detected in the ACIS-S3 chip fall in those two regions. We therefore limited our analysis to the cluster HUGS source catalogue. Among the optical sources, we could select only nine that satisfy the condition of being the only ones

<sup>1</sup> <http://groups.dfa.unipd.it/ESPG/treasury.php>

**Table 1.** Log of the X-ray observations of M22 analysed in this work.

	Obs.	Start Time (UT)	Stop Time (UT)	Exposure Time (s)
<i>XMM-Newton</i>	0112220201	2000-09-19 22:05:00	2000-09-20 09:31:56	41216
<i>Chandra</i>	5437	2005-05-24 21:22:27	2005-05-25 02:12:40	15819
	14609	2014-05-22 19:40:24	2014-05-23 20:00:44	84864
<i>Swift/XRT</i>	34847001	2017-03-07 06:34:57	2017-03-07 09:03:36	2412
	34847002	2017-03-23 15:07:57	2017-03-23 19:09:39	2550
	34847003	2017-04-03 23:58:57	2017-04-04 05:22:41	1988
	34847004	2017-05-02 03:55:57	2017-05-02 23:37:16	2272
	34847005	2017-05-16 21:24:57	2017-05-17 00:07:26	1377
	34847006	2017-05-30 06:05:57	2017-05-30 10:24:12	2926
	34847007	2017-06-13 19:06:57	2017-06-13 21:36:51	3011
	34847008	2017-06-27 05:14:57	2017-06-28 00:30:46	2801
	34847009	2017-07-11 10:18:57	2017-07-11 16:41:07	2821
	34847010	2017-07-25 01:22:57	2017-07-26 00:34:23	2693
	34847011	2017-08-08 03:15:57	2017-08-08 16:59:13	3074
	34847012	2017-08-22 11:54:57	2017-08-22 20:47:36	1529
	34847013	2017-08-25 11:29:57	2017-08-25 13:13:34	925
	34847014	2017-09-05 13:53:57	2017-09-05 17:57:26	1086
	34847015	2017-09-08 13:16:57	2017-09-08 15:50:11	2580
	34847016	2017-09-19 20:48:57	2017-09-20 00:23:58	2580
	34847017	2017-10-03 03:26:56	2017-10-03 13:40:01	2878
	34847018	2017-10-18 00:14:57	2017-10-18 23:29:29	2989
	34847019	2017-10-31 04:04:57	2017-10-31 06:33:44	2221
	10376001	2018-02-16 02:20:57	2018-02-17 22:34:10	8397
	10376002	2018-03-15 10:04:56	2018-03-16 00:43:10	3881
	10376003	2018-03-16 20:32:57	2018-03-17 02:13:05	5305
	10376004	2018-04-15 02:02:57	2018-04-15 10:52:39	5433
	10376005	2018-04-18 09:53:57	2018-04-18 13:45:06	1958
	10376006	2018-05-15 07:10:57	2018-05-15 11:24:38	1645
	10376007	2018-05-16 07:03:57	2018-05-17 00:06:40	7456
10376008	2018-06-15 10:51:57	2018-06-15 19:39:23	9792	
10376009	2018-07-15 01:53:56	2018-07-15 17:07:35	9816	

bright (typically  $F814W < 18$  mag) within a small ( $\lesssim 1.2''$  major axis)  $1\sigma$  error ellipse. In most cases, the optical source was the only one (when more than one bright source was present the corresponding X-ray source was disregarded). In just a few cases, two or three much fainter stars were present. The association was done irrespective of being cluster members or not (see also Section 5). Among the nine sources, eight are within the cluster core and one within the half-mass radius. One of them corresponds to the source labelled CV1 by Webb & Servillat (2013), classified as a cataclysmic variable through the study of its the X-ray emission and optical spectrum. Its position matches the star R0047833 in the HUGS catalogue. We use the CIAO tools `wcs_MATCH`, to perform a cross-matching through a translation (`METHOD=TRANS`), and `wcs_UPDATE` to upgrade the aspect solution file, the `level=2` event files and the list of the detected sources. We find an average systematic shift of  $+0.071''$  in R.A. and of  $-0.634''$  in Dec., with an rms value of  $0.3''$ . Applying this correction, we then find the X-ray source at R.A.=18:36:25.5 and Dec.=−23:54:52.1. The radio MSP M22A lies well inside the  $1\sigma$  X-ray error ellipse (see Fig. 3). Hence, the detected X-ray source can be confidently seen as the counterpart of the radio MSP M22A.

#### 4 X-RAY DATA ANALYSIS

We find 5.5 and 11.8 net counts for ObsID 5436 and ObsID 14609, respectively. The net count rates are then  $(4.1 \pm 1.8) \times 10^{-4}$

cts  $s^{-1}$  (ObsID 5436) and  $(1.8 \pm 0.4) \times 10^{-4}$  cts  $s^{-1}$  (ObsID 14609). We verified the consistency of the two count rates by a Poissonian ratio test. We tested the null hypothesis probability of the first rate being equal to the second. The resulting *p-value* of 0.1 does not constitute a strong evidence against the null hypothesis probability, which is not rejected. We concluded that there is not any statistically significant variability between the two observations. We also investigated the distribution of the arrival times of the detected photons with energies up to 8 keV, considering an extraction region of  $1''$ , for both the 2005 and 2014 *Chandra* observations. We do not detect any clear modulation linked to the orbital period ( $P_b = 0.2028278011(3)$  days), possibly due to the very low statistics.

We extracted a source spectrum from each observation, selecting a circular area centered at the best-fit position returned by `WAVDETECT` using a radius of  $1''$  and binning the spectrum to have at least 1 count per noticed bin. We used `XSPEC`, version 12.9, for spectral analysis. Due to the low number of counts, we used the C-statistic (Cash 1979). Errors are given at  $1\sigma$  confidence level, if not stated otherwise.

Since no statistically significant variability is present in the two observations, we fitted the two spectra together, in the energy range 0.5–6 keV, adopting two alternative models: an absorbed power law and an absorbed black-body. We used the `TBABS` (in `XSPEC`) component for the interstellar neutral absorption, setting the element abundances from Wilms et al. (2000) and the cross-sections from

Verner et al. (1996), and the equivalent hydrogen column density value  $N_{\text{H}}$  fixed to  $0.197 \times 10^{22}$  atoms  $\text{cm}^{-2}$  (Cheng et al. 2018).

The power law model gave a photon index  $\Gamma = 1.5^{+0.7}_{-0.6}$ , while the black-body model (BBODYRAD in XSPEC) has a best-fitting temperature of  $0.8 \pm 0.4$  keV. To evaluate the fit goodness, we iterated over 1000 Monte Carlo simulated spectra, within XSPEC. We obtained the 0.30% of realisations with lower C-statistic values than the best fit ones, in both cases. Hence, the models are both acceptable, though the very low number of counts does not allow us to discriminate between them.

The unabsorbed fluxes, calculated in the energy range 0.5–8 keV, are  $2.3^{+1.2}_{-0.6} \times 10^{-15}$  erg  $\text{cm}^{-2}$   $\text{s}^{-1}$  for the power law model and  $1.8^{+1.2}_{-0.9} \times 10^{-15}$  for the black-body model. These values give an X-ray luminosity of  $2.8 \times 10^{30}$  erg  $\text{s}^{-1}$  for the power law model and  $2.2 \times 10^{30}$  erg  $\text{s}^{-1}$  for the black-body model, respectively, assuming a distance of 3.2 kpc (see Table 2). We obtain a X-ray flux slightly lower than that reported by Webb & Servillat (2013) of  $5.2 \times 10^{-15}$  erg  $\text{cm}^{-2}$   $\text{s}^{-1}$  ( $1\sigma$  error). This is due to the different power law slope assumed by Webb & Servillat (2013) in their analysis (2.1 instead of 1.5). However, by fitting the 2005 spectrum with a fixed the power law slope at 2.1, we obtained a slightly higher, but still consistent, unabsorbed flux, equal to  $9.1 \times 10^{-15}$  erg  $\text{cm}^{-2}$   $\text{s}^{-1}$ , in the energy range 0.5–8 keV.

The archival *XMM-Newton* and *Swift* observations have over-all exposure times of  $\sim 41$  ks and  $\sim 96$  ks. Using the NASA's HEASARC tool WEBBPIIMMS<sup>2</sup>, we estimated the expected count rates for the EPIC instruments and *Swift*/XRT observations. We converted the mean flux of the two *Chandra* observations derived from the power law model into count rates, obtaining  $5.4 \times 10^{-4}$  cts  $\text{s}^{-1}$  for *XMM*/EPICs and  $4.4 \times 10^{-5}$  cts  $\text{s}^{-1}$  for *Swift*/XRT. The count rate thresholds ( $3\sigma$ ) for *XMM-Newton* observation and for the stacked *Swift* one are of  $6.9 \times 10^{-4}$  cts  $\text{s}^{-1}$  and  $8.5 \times 10^{-5}$  cts  $\text{s}^{-1}$ . Hence, the source flux is well below the threshold of detectability in both the data sets. Moreover the PSFs are far larger (nominally  $15''$  at 1 keV for *XMM-Newton* and  $18''$  at 1.5 keV for *Swift*, against  $0.5''$  of *Chandra*), so that M22A, which is in the cluster core, cannot be resolved with respect to the closest and brightest source (source 2 of Webb & Servillat (2013), see also Fig. 1).

However, since it cannot be excluded that the source could have undergone a change of luminosity in the recent past, we inspected the *Swift*/XRT images one by one, with XIMAGE, using a signal to noise ratio threshold of three. Once we checked out that the source was never detected, we looked for its X-ray emission in the stacked XRT image. For purpose of comparison with Webb et al. (2004), we also performed a source detection on the *XMM-Newton* combined EPIC/pn and EPIC/MOS images, using the tool EDETECT\_CHAIN, with the appropriate Energy Conversion Factor (ecf) values of the medium filter configuration. In neither case we detect any source at the radio position of the MSP, as the source have remained below the threshold sensitivity of the two instruments. The detection pipelines, indeed, identified sources with fluxes down to  $9 \times 10^{-15}$  erg  $\text{cm}^{-2}$   $\text{s}^{-1}$  for *XMM-Newton* and to  $1.1 \times 10^{-14}$  erg  $\text{cm}^{-2}$   $\text{s}^{-1}$  for *Swift*. The sensitivity thresholds, together with the larger PSFs, justify the lack of detection of M22A.

## 5 OPTICAL OBSERVATIONS

We searched for the optical counterpart of the radio MSP M22A using *HST* images and the astrophotometric catalogue of M22 (Nardiello et al. 2018) from the treasury project HUGS (Pitto et al. 2015). M22 has been imaged in several filters with the WFC3/UVIS (F275W, F336W, F438W) and ACS/WFC cameras (F606W and F814W). We inspected the stacked images in all the five filters, against the astrophotometric catalogue that also provides probability membership for each detected star (see Nardiello et al. 2018, for details). Within the accuracy of the radio position provided by Lynch et al. (2011), no optical counterpart is detected. The two closest cluster member stars, catalogued as R0039501 ( $m_{814W} = 20.59(5)$ ) and R0002743 ( $m_{814W} = 17.254(7)$ ) in the HUGS project list, are found at much larger distance of  $0.197''$  and  $0.237''$ , respectively. The optical positions of these two stars are very accurate,  $0.0014''$  and  $0.0024''$  respectively (Nardiello, private communication), and therefore we exclude them as possible counterparts. We infer a  $3\sigma$  upper limit at the position of the radio source of  $m_{F606W} \geq 25.6$  mag and  $m_{F814W} \geq 24.7$  mag in the stacked long exposures in these two filters. The stacked astrometrically corrected image in the F814W filter is shown in Fig. 3, together with the radio position of the MSP from Lynch et al. (2011) and with the X-ray position of our detection in the latest *Chandra* dataset.

While we are confident that no optical counterpart is detected for the radio source M22A in the *HST* images, we note that *Chandra* error region in Fig. 3 shows four or five optical sources within the  $1\sigma$  region and tens of sources at the  $3\sigma$  level. A scrupulous inspection of the closest optical sources in the Colour-Magnitude diagram revealed no bona-fide candidate to a possible red straggler source (Geller et al. 2017), which are sometimes associated to quiescent X-ray binary systems (Shishkovsky et al. 2018). We therefore believe that the source identified in the *Chandra* data is the X-ray counterpart of the radio MSP M22A and consequently none of the optical sources in its error ellipse can be safely associated to the X-ray source.

## 6 THE $\gamma$ -RAY EMISSION FROM M22

Based on the  $\gamma$ -ray association to the GC M22 by Zhou et al. (2015), we checked whether this  $\gamma$ -ray source is compatible with the M22A position by using the latest *Fermi*-LAT catalogues. We found in the 4-year catalogue (3FGL, Acero et al. 2015) that the source 3FGL J1837.3–2403 is positionally consistent with the emission detected by Zhou et al. (2015), but the MSP M22A is off from the 95% error region (Fig. 4, yellow ellipse)<sup>3</sup>. The 95% error ellipse touches the half-mass radius of the cluster, but does not cover the cluster core. 3FGL J1837.3–2403 showed a power law spectrum with photon index  $2.40 \pm 0.14$  and a flux in the 0.1–100 GeV range of  $(8.7 \pm 1.7) \times 10^{-12}$  erg  $\text{cm}^{-2}$   $\text{s}^{-1}$ , consistent with the best fit power law by Zhou et al. (2015). The corresponding  $\gamma$ -ray luminosity is  $(10.6 \pm 2.1) \times 10^{33}$  erg  $\text{s}^{-1}$ , for a distance of 3.2 kpc. 3FGL J1837.3–2403 appears rather stable, as also indicated by the low variability index of 43.73 reported in the catalogue (see also Acero et al. 2015, for details on variability).

From the inspection of the preliminary 8-yr *Fermi*-LAT source list (FL8Y), we found that 3FGL J1837.3–2403 is associated to FL8Y J1836.7–2355, whose detection is at  $6.45\sigma$  and at only  $5.1'$

<sup>2</sup> <https://heasarc.gsfc.nasa.gov/cgi-bin/Tools/w3pimms/w3pimms.pl>

<sup>3</sup> The other MSP identified by Lynch et al. (2011), M22B, does not fall in the 95% 3FGL J1837.3–2403 error ellipse either.



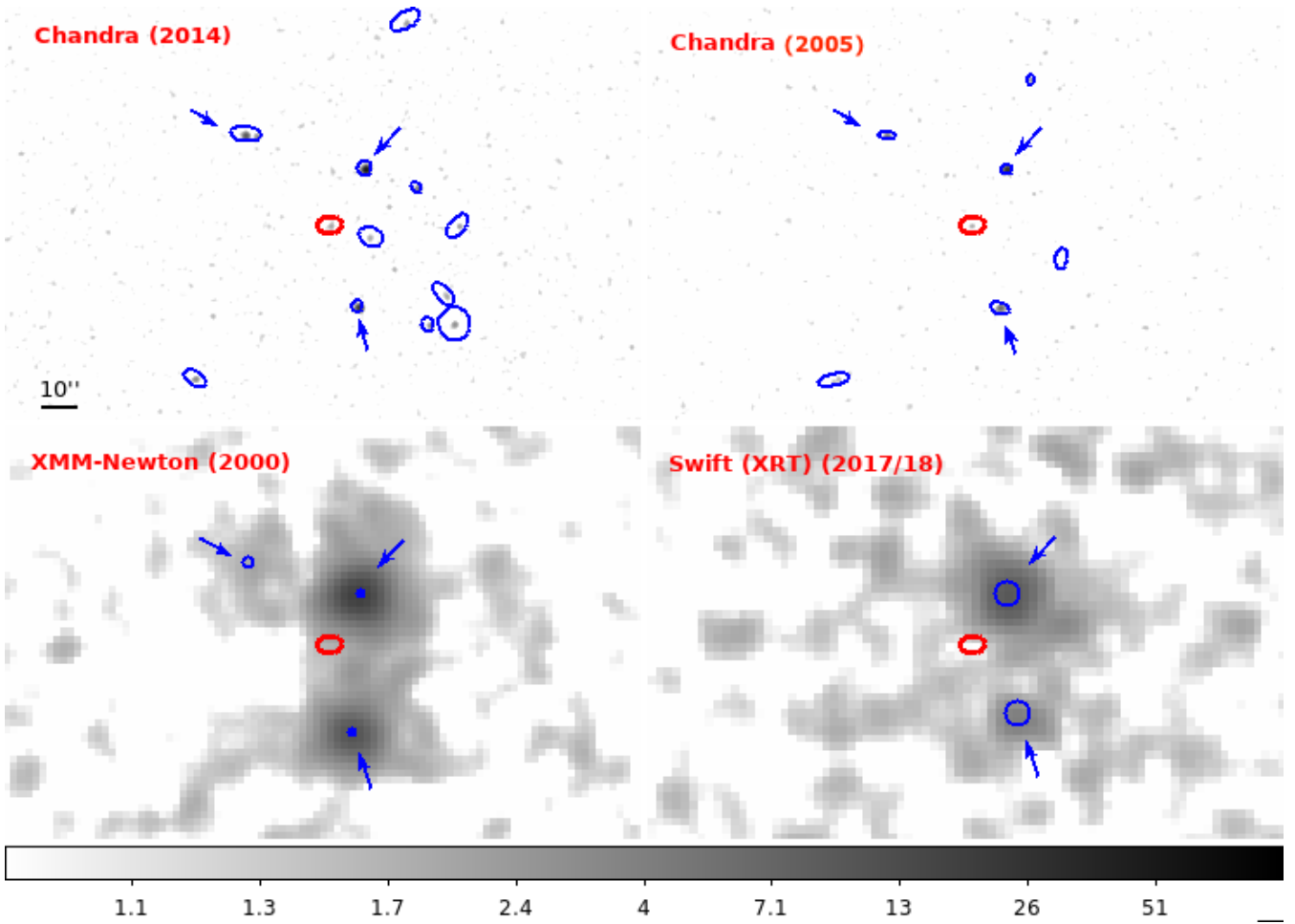


**Figure 1.** X-ray images of *Chandra* ObsID 14609 (top left panel) and 5437 (top right panel), of *XMM-Newton* obs. (bottom left panel) and of the stacked *Swift*-XRT observations (bottom right panel). The red ellipse corresponds to the position of M22A in the longest *Chandra* obs. (14609), the blue circles/ellipses indicate the other detected X-ray sources. The dimensions of each ellipse in *Chandra* observations correspond to a  $3\sigma$  positional error as given by the detection pipeline, the dimension of the circles of *Swift* observations are the catalogued positional errors (<http://xmm-catalog.irap.omp.eu/>). The blue arrows point to the most luminous sources close to M22A detected in almost all the data sets.

**Table 2.** Best-fit values of the simultaneous fit of the spectra of M22A from *Chandra* ObsID 5437 and 14609. The fit was performed with the C-statistic, the errors are at  $1\sigma$  confidence level and the goodness was calculated over 1000 Monte Carlo simulations on the ObsID 14609.

Model	$\Gamma$	$kT$ (keV)	$R_{eff}$ ( $10^{-3}$ km)	Unabs. Flux [0.5-8 keV] ( $10^{-15}$ erg $\text{cm}^{-2}$ $\text{s}^{-1}$ )	$L_X$ [0.5-8 keV] ( $10^{30}$ erg $\text{s}^{-1}$ )
POWER-LAW	$1.5^{+0.7}_{-0.6}$			$2.3^{+1.2}_{-0.6}$	$2.8^{+1.5}_{-0.9}$
BBODYRAD		$0.8 \pm 0.4$	$6.5^{+7.5}_{-3.8}$	$1.8^{+1.2}_{-0.9}$	$2.2^{+2.0}_{-1.1}$

from the cluster centre. Though the 95% error ellipse is smaller (Fig. 4, green ellipse), it includes both the radio positions of the two MSPs M22A and M22B and obviously precludes a clear association to any of them.

While the present work was under review stage, the final 8-year catalogue (4FGL, [The Fermi-LAT collaboration 2019](#)) was officially released. The new release refines the preliminary position of the FL8Y list. The closest source to M22 is 4FGL J1836.8–2354, detected at  $8.2\sigma$ , at a distance of almost  $6'$  from the cluster centre. Its 95% error region barely touches the cluster core and does not encompass M22A, neither at the radio or X-ray position, though

it is very close (see Fig. 4, red ellipse)<sup>4</sup>. In the 4FGL catalogue the source spectrum is found to be best fit with a log-normal representation (LogParabola)<sup>5</sup>. The significance of the fit of a LogParabola over a power law is  $4.2\sigma$ . The energy flux in the 0.1–100 GeV range is  $(4.1 \pm 0.9) \times 10^{-12}$  erg  $\text{cm}^{-2}$   $\text{s}^{-1}$  with a corresponding  $\gamma$ -ray lumi-

<sup>4</sup> The 95% elliptic region of 4FGL J1836.8–2354 does not encompass M22B either.

<sup>5</sup> See [https://fermi.gsfc.nasa.gov/ssc/data/access/lat/8yr\\_catalog/](https://fermi.gsfc.nasa.gov/ssc/data/access/lat/8yr_catalog/).

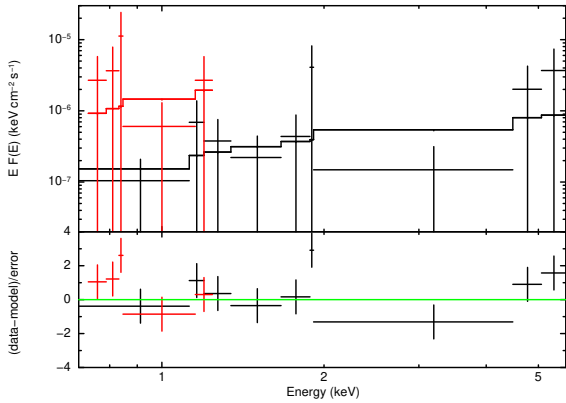


**Figure 2.** Simultaneous fit of *Chandra* obs. ID 14609 (black) and obs. ID 5437 (red) with a power law plus absorption model and residuals as (data-model)/error where error is calculated as the square root of the model predicted number of counts, in the energy range 0.5-6 keV.

nosity of  $(5.0 \pm 1.1) \times 10^{33} \text{ erg s}^{-1}$ . The difference in flux between the 3FGL and 4FGL catalogues is consistent within  $2\sigma$ .

## 7 DISCUSSION

In this work, we present a comprehensive study of the radio MSP M22A, located in the GC M22, from multiwavelength observations. We search for X-ray emission from M22A, taking into account all the available X-ray observations within the last two decades. Using the most recent *Chandra* observation of 2014, we detect an X-ray source whose  $1\sigma$  positional uncertainty encompasses the radio source M22A and therefore we ascribe it as the X-ray counterpart of the radio MSP. Thanks to its  $\sim 85$  ks of exposure time, the *Chandra* observation allows us to investigate the spectral shape and to determine the X-ray luminosity of the pulsar. We do not detect any X-ray emission from M22A in either *XMM-Newton* or *Swift*/XRT pointings; the *Swift* monitoring campaign of the cluster, with one or two visits per month, shows that M22A remains likely around, or below, the luminosity derived in the *Chandra* observations.

We studied the X-ray spectrum of M22A by using the data from the two *Chandra* observations. We considered two possible scenarios: a non-thermal emission, originating from an intrabinary shock produced between the powerful pulsar wind and that from the companion star (Romani & Sanchez 2016, Wadiasingh et al. 2017), and a thermal emission, which could originate in the polar caps of the NS, where the infall of relativistic particles keeps heating the pulsar surface (Gentile et al. 2014). Both the emission mechanisms are discussed below.

The X-ray spectrum can be reasonably fitted with a relatively hard power-law ( $\Gamma \sim 1.5$ ) which could hint at a non-thermal origin and favours the intrabinary shock scenario. In fact, the X-ray emission from the shock is expected to be hard with a power law shape with index 1.1 – 1.2 (Becker & Trümper 1999, Zavlin 2007). The X-ray flux and spectrum is also expected to be variable at the binary orbital period, as indeed found in most systems (Bogdanov

et al. 2005, Gentile et al. 2014, de Martino et al. 2015, Roberts et al. 2015). Unfortunately, due to the low statistics, we could not infer any orbital modulation. We compare the photon index of M22A with those presented by Arumugasamy et al. (2015) for a sample of black widow pulsars (see also Gentile et al. 2014) and those of Linares (2014) for a sample of redbacks (see also Roberts et al. 2015, Strader et al. 2019), as shown in Fig. 5 (top panel). Though the photon index of M22A is poorly constrained, it is consistent with similar hard values found in a number of black widows and in all redbacks.

Thermal emission is often observed from faint MSPs, where the total power generated is  $\log_{10}(L_X) = 30-32 \text{ erg s}^{-1}$  (Bogdanov et al. 2006, Forestell et al. 2014, Bhattacharya et al. 2017) and the magnetic field is low, typically  $B \lesssim 10^9 \text{ G}$  (Zavlin et al. 1996, Heinke et al. 2006). The intensity of the magnetic field at the surface of the NS, in the simple case of a magnetic dipole, is given by  $B_{\text{surf}} = 3.2 \times 10^{19} (P\dot{P})^{1/2} \text{ G}$  (Manchester & Taylor 1977), where  $P$  and  $\dot{P}$  are respectively the spin period and the spin-down rate of the NS. From Lynch et al. (2011),  $P \approx 3.35 \text{ ms}$  and  $\dot{P} \approx 5.36 \times 10^{-21} \text{ ss}^{-1}$ , being  $\dot{P}$  the intrinsic spin-down of the pulsar, disentangled from the effect due to the potential of the Galaxy and of the proper motion of the cluster (Lynch et al. 2011, formula 9). Hence,  $B_{\text{surf}} \sim 1.4 \times 10^8 \text{ G}$ , implying that the contribution of a thermal emission cannot be excluded.

The X-ray spectrum, indeed, could be equally described by a black-body with temperature of  $0.8 \pm 0.4 \text{ keV}$ . It is perfectly consistent with the temperatures of other samples of X-ray pulsars (see, for instance, Bogdanov et al. (2006) and Bhattacharya et al. (2017) for a spectral analysis of the MSPs of the GC 47 Tucanae).

To argue more deeply about the thermal scenario, we can use the correlation between the X-ray luminosity and the rotational energy loss rate ( $\dot{E} = 4\pi^2 I \dot{P} / P^3$ ), which is equal to  $\sim 5.6 \times 10^{33} \text{ erg s}^{-1}$  for M22A. We compare our result with a sample of 24 MSPs (Gentile et al. 2014) in Fig. 6. Under the hypothesis that the rotational energy loss rate is converted in X-ray thermal emission from the polar caps with an efficiency of 0.1% (Pavlov et al. 2007) (solid line in Fig. 6), the thermal conversion mechanism would seem to be plausible for M22A. However, we underline that the best-fit value of the radius of the emitting polar cap,  $R_{\text{eff}} = 6.5_{-4}^{+8} \text{ m}$  (Tab. 2), is unrealistically small.

We derive an X-ray luminosity of  $(2 - 3) \times 10^{30} \text{ erg s}^{-1}$ , for the black-body and the power law models, respectively, in the energy range 0.5–8 keV. These values are consistent with the ones typically found for GC X-ray sources ( $L_X \sim 10^{30} - 10^{31} \text{ erg s}^{-1}$ ) (Bogdanov et al. 2006). On the base of the X-ray luminosity, we try to discriminate whether M22A is more likely a black widow or a redback. For this purpose, we made a comparison between the X-ray luminosities of the black widow pulsars from Arumugasamy et al. (2015) and of the redbacks from Linares (2014), as shown in the bottom panel of Fig 5 (for a wider sample consider also sources from Gentile et al. (2014), Roberts et al. (2015) and Strader et al. (2019)). Black widows luminosities are in the range  $\log_{10}(L_X) = 30.2 - 31.3 \text{ erg s}^{-1}$ , while redbacks luminosities seem to be systematically higher, in the range  $\log_{10}(L_X) = 31.5 - 33.7 \text{ erg s}^{-1}$ . With a value of  $\log_{10}(L_X) = 30.5 \text{ erg s}^{-1}$ , in the range 0.5–10 keV, M22A is more consistent with black widows rather than with redbacks.

The persistent low X-ray flux does not favour accretion of matter from the companion star. The low companion mass and relatively large orbital period seem to indicate that mass accretion in this system is unlikely. The mass function of  $2.6 \times 10^{-6}$  indicates

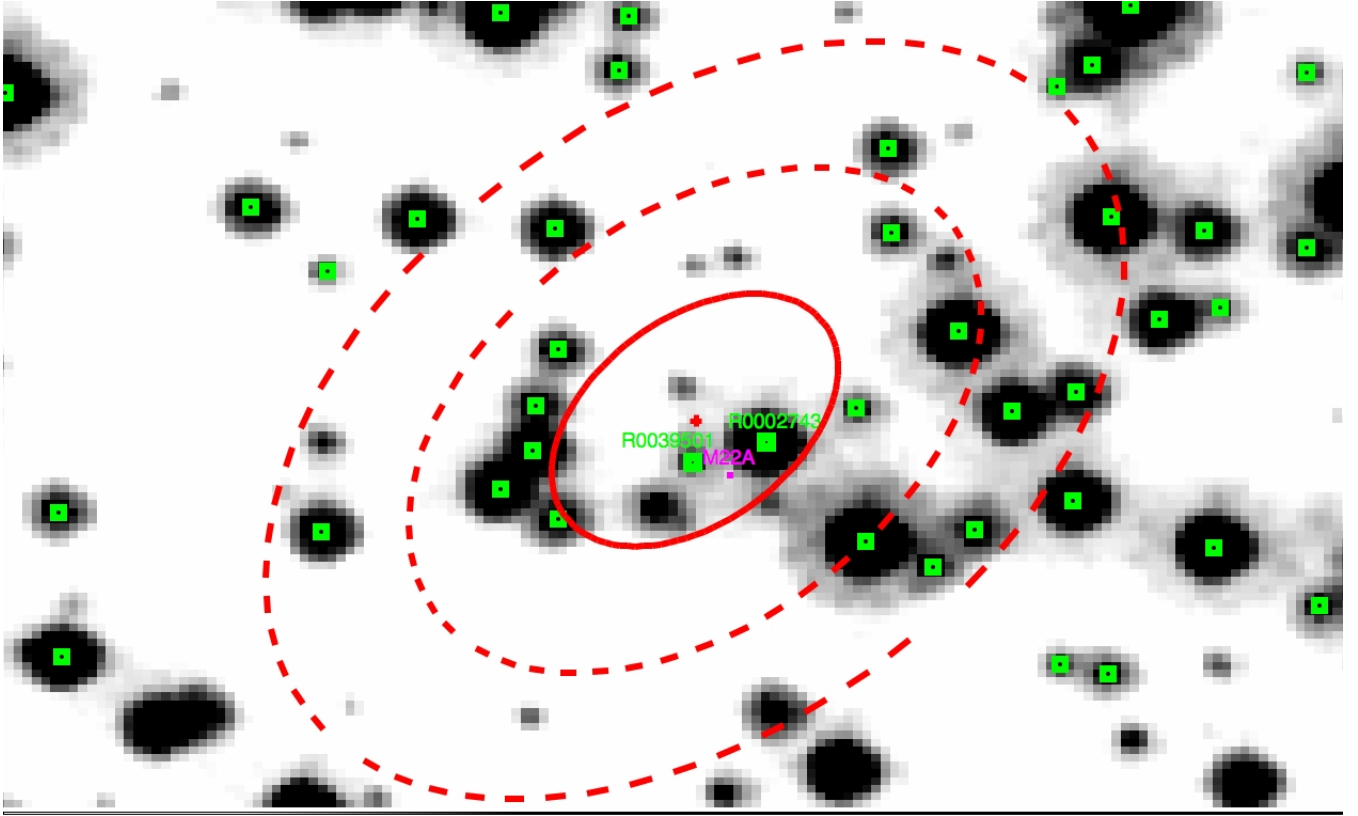


**Figure 3.** The  $8'' \times 4''$  enlarged region of the *HST* stacked ACS image in the F818W filter (Nardiello et al. 2018) around M22A. North is up, East is left. M22A is marked in magenta. The X-ray  $1\sigma$  error ellipse is reported with a red line, the  $2\sigma$  and  $3\sigma$  error ellipses with red dashed lines. The green boxes mark the optical stars belonging to the M22 cluster with probability membership  $> 80\%$ . The two cluster stars, labelled R0039501 and R0002743, have accuracies that rule out any association with M22A.

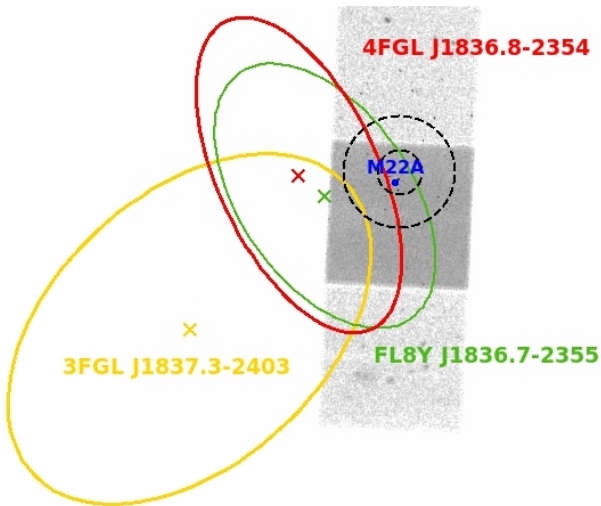


**Figure 4.**  $\gamma$ -ray sources and 95% error ellipses from the 3FGL (in yellow, Acero et al. 2015), the preliminary FL8Y (in green) and the 4FGL (in red, The Fermi-LAT collaboration 2019) catalogues of *Fermi*-LAT. The blue dot marks the radio position of the MSP M22A, while the black dashed circles the core radius (inner circle) and the half-mass radius (outer circle) of M22.

a companion star of mass  $M_2 = 0.017 M_\odot$  for  $i = 90^\circ$  (Lynch et al. 2011) and  $M_2 = 0.22 M_\odot$  for  $i = 5^\circ$ . We exclude lower angles, being the probability of observing a binary system with an inclination  $i < 5^\circ$  equal to  $1 - \cos(i) \approx 0.4\%$  (Lorimer & Kramer 2004). Using  $M_2 = 0.22 M_\odot$  as an upper limit, we consider a Roche-lobe overflow as possible mechanism of mass transfer. In this case the secondary star radius  $R_2$  must be at least of the same order of magnitude of its Roche lobe radius  $R_L$ , therefore it is sufficient to compare the two radii  $R_2$  and  $R_{L,2}$ . The size of the Roche lobes is  $R_{L,2} = 0.49q^{2/3} / [0.6q^{2/3} + \ln(1 + q^{1/3})]a$  (Eggleton 1983), where  $q$  is the ratio between  $M_2$  and  $M_1$ , the mass of the primary star, and of the orbital separation  $a$ . We adopt a mass of  $1.4 M_\odot$  for the NS and the range  $0.02\text{--}0.2 M_\odot$  for the companion, according to the possible inclinations of the system. Using the third Kepler’s law we derive an orbital separation  $a$  in the range  $(1.14\text{--}1.16) \times 10^6$  km and, hence,  $R_{L,2} = (1.2\text{--}2.7) \times 10^5$  km ( $0.18\text{--}0.39 R_\odot$ ). On the other hand, an estimation of  $R_2$  can be made according to the mass-radius relationships for low mass stars and sub-stellar objects by Chabrier et al. (2000) (see their Table 5); for an “old” object, with an age of  $\approx 10$  Gyr and a mass between  $0.05$  and  $0.1 M_\odot$ , the radius ranges between  $0.08$  and  $0.12 R_\odot$ , which is about the Jupiter radius. Since  $R_2 < R_{L,2}$ , the accretion of matter onto the NS through Roche-lobe overflow is ruled out.

However, it cannot be excluded that the companion star is out of thermal equilibrium and bloated with respect to its main sequence configuration (see, e.g., King 1988). In this case, the companion star can be close to fill its Roche lobe and can transfer

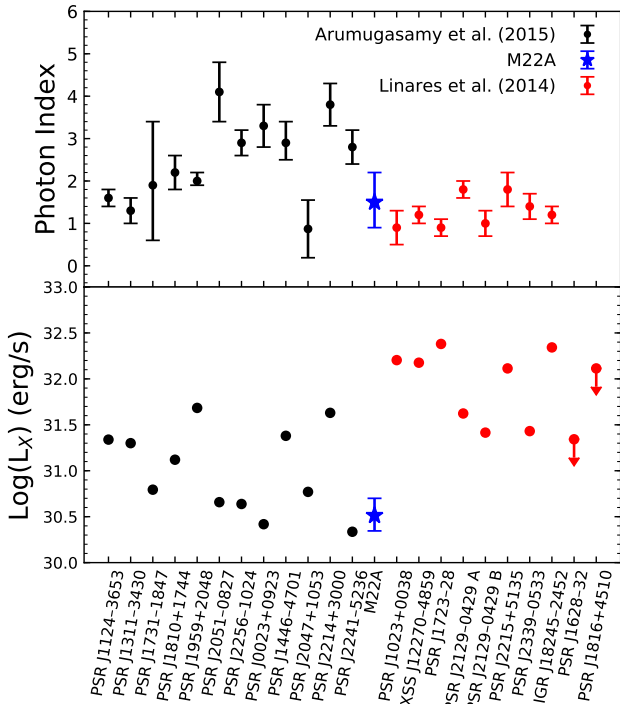


**Figure 5.** Photon indices (*top panel*) and X-ray luminosities in the energy range 0.5–10 keV (*bottom panel*) of a sample of black widows (black) from Arumugasamy et al. (2015), redbacks (red) from Linares (2014) and our derived values for M22A (blue star).

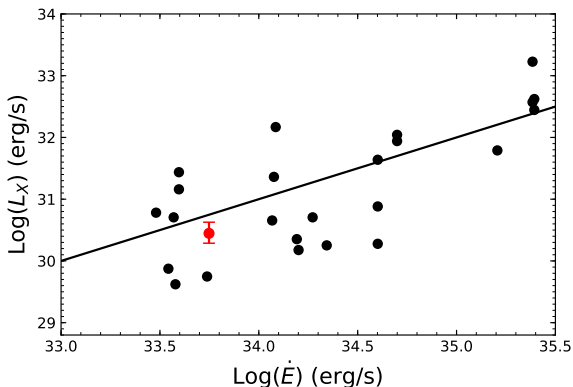


**Figure 6.** Luminosity versus spin-down energy loss rate  $\dot{E}$  for 24 X-ray detected MSPs (black circles), from Gentile et al. (2014). The red dot stands for M22A. Luminosities are in the 0.3–8.0 keV range, while the line represents 0.1% efficiency.

or loose mass (as it happens in red-backs and black widows) thanks also to the pulsar irradiation. In any case, we do not expect accretion in this phase of the system since the radiation pressure from the pulsar may be able to expel the mass transferred by the companion star out of the system (see, e.g., Burderi et al. 2001).

Even in the case of a lack of detection of an optical counterpart, we can derive some constraints on the nature of the companion

of M22A. We compare the expected magnitudes for the case of maximum radii, i.e. Roche-lobe filling between 0.18 and 0.39  $R_{\odot}$ , adopting temperatures up to 3400 K. Here we note that no brown dwarf is expected to have temperatures above 3000 K and radius larger than 0.2  $R_{\odot}$  even at 0.1 Gyr (Chabrier et al. 2000). The upper limits in the F606W and F814W filters derived from *HST*, once converted into the Johnson-Cousin system (Siriani et al. 2005) and adopting an interstellar extinction  $E(B-V)=0.34$  (Alonso-García et al. 2012) and the distance of 3.2 kpc, give absolute magnitudes of 12.5 and 11.6 in the V and I bands, respectively. These values are well above the evolutionary sequences of brown dwarfs by more than 3 mag in V and 1 mag in I (Chabrier et al. 2000). For  $R_2$  between 0.18  $R_{\odot}$  and 0.39  $R_{\odot}$  and  $T_{\text{eff}} = 3400$  K, the expected magnitudes are  $V=13.3-10.8$  mag and  $I=10.8-8.6$  mag, respectively. On the other hand, the limits in the V and I bands would correspond, for a similar temperature, to a stellar radius of 0.23  $R_{\odot}$  and 0.16  $R_{\odot}$ . In the case of Roche-lobe filling, i.e.  $R_2 = R_{L2}$ , adopting again 1.4  $M_{\odot}$  for the NS, these radii would correspond to masses between 0.04 and 0.014  $M_{\odot}$ , respectively. Releasing the Roche-lobe filling condition, the magnitude limits and thus the corresponding upper limits to the radii give a main sequence star of 0.2  $M_{\odot}$  and 0.1  $M_{\odot}$  respectively (Baraffe et al. 2015). Therefore, although tentative, these estimate appears to rule out a companion with a mass above 0.1–0.2  $M_{\odot}$ . According to the recent study of Strader et al. (2019), redback companions have median masses of  $0.36 \pm 0.04 M_{\odot}$ , with a scatter of  $\sigma = 0.15 \pm 0.04 M_{\odot}$ . Thus, our analysis may favour a black widow binary, in agreement with the interpretation of Lynch et al. (2011).

Concerning the  $\gamma$ -ray emission, the new position and uncertainty in the 8-year catalogue seem to exclude the contribution of the two MSPs to the  $\gamma$ -ray emission of 4FGL J1836.8–2354, although the 95% error ellipse is only slightly offset from the two radio sources. The number of MSPs expected in the cluster can be estimated as  $N_{\text{MSP}} = L_{\gamma} / \langle \dot{E} \rangle \langle \eta_{\gamma} \rangle$  (Abdo et al. 2010), where  $L_{\gamma}$  is the  $\gamma$ -ray luminosity of the cluster,  $\langle \dot{E} \rangle$  is the average power loss during the spin down of MSPs and  $\langle \eta_{\gamma} \rangle$  is the average conversion efficiency of the spin down power into  $\gamma$ -ray radiation. Assuming  $\langle \dot{E} \rangle = (1.8 \pm 0.7) \times 10^{34}$  erg s<sup>-1</sup>,  $\langle \eta_{\gamma} \rangle = 0.08$  (Abdo et al. 2010) and  $L_{\gamma} = 5 \times 10^{33}$  erg s<sup>-1</sup>, we obtain  $N_{\text{MSP}} \simeq 4$ , i.e. we expect that the  $\gamma$ -ray emission seen from *Fermi* is the cumulative contribution of at least 4 MSPs. With only 2 radio MSPs detected in M22 so far, we are unable to assess their true contribution. The curved  $\gamma$ -ray spectrum, as reported in the 8-year *Fermi*-LAT catalogue, may be also compatible with an origin from pulsars (The *Fermi*-LAT collaboration 2019).

## 8 CONCLUSIONS

We have carried out a search for the X-ray, optical and  $\gamma$ -ray counterparts of the radio MSP M22A, detected by Lynch et al. (2011). We find persistent X-ray emission in two *Chandra* observations, made in 2005 and 2014 respectively. The X-ray spectrum is well modeled either with a hard power law, with a photon index of  $\sim 1.5$ , or with a black-body model with a temperature of  $\sim 0.8$  keV. However, the latter gives an unrealistic value of the effective polar cap radius, which makes the intrabinary shock scenario more likely than thermal emission from the NS surface. No optical counterpart has been found and the inferred upper limits on the magnitudes allow us to derive an upper limit on the mass of the companion star of



$0.2 M_{\odot}$ , typical for black widow systems. No  $\gamma$ -ray emission from M22 core is found in the latest *Fermi*-LAT catalogues.

Further studies of this X-ray source can be made with new generation of satellites, like *eRosita*, planned to flight in 2019, *eXTP*, planned to flight earlier than 2025, or *ATHENA*, whose launch is scheduled in 2030s, thus allowing more constraints on the nature of this system.

## ACKNOWLEDGEMENTS

We gratefully thank D. Nardiello and G.P. Piotto for providing positional accuracies and background values of the *HST* images within the HUGS project. Authors acknowledge financial contribution from the agreement ASI-INAF n.2017-14-H.O. AD acknowledges support from the ASI Grant I/004/11/1. DDM acknowledges financial contribution from “Towards the SKA and CTA era” (P.I. M. Giroletti) and RI and TDS from the research grant “iPeska” (P.I. A. Possenti), both funded under the INAF national call Prin-SKA/CTA approved with the Presidential Decree 70/2016. RI and TDS acknowledge also financial contribution from the HERMES Project, funded by the Italian Space Agency (ASI) Agreement n. 2016/13 U.O.

## REFERENCES

- Abdo A. A., et al., 2010, *A&A*, **524**, A75
- Acero F., et al., 2015, *ApJS*, **218**, 23
- Alonso-García J., Mateo M., Sen B., Banerjee M., Catelan M., Minniti D., von Braun K., 2012, *AJ*, **143**, 70
- Alpar M. A., Cheng A. F., Ruderman M. A., Shaham J., 1982, *Nature*, **300**, 728
- Archibald A. M., et al., 2009, *Science*, **324**, 1411
- Arumugasamy P., Pavlov G. G., Garmire G. P., 2015, *ApJ*, **814**, 90
- Baraffe I., Homeier D., Allard F., Chabrier G., 2015, *A&A*, **577**, A42
- Bassa C. G., et al., 2014, *MNRAS*, **441**, 1825
- Becker W., Trümper J., 1999, *A&A*, **341**, 803
- Bhattacharya D., van den Heuvel E. P. J., 1991, *Phys. Rep.*, **203**, 1
- Bhattacharya S., Heinke C. O., Chugunov A. I., Freire P. C. C., Ridolfi A., Bogdanov S., 2017, *MNRAS*, **472**, 3706
- Bogdanov S., Grindlay J. E., van den Berg M., 2005, *ApJ*, **630**, 1029
- Bogdanov S., Grindlay J. E., Heinke C. O., Camilo F., Freire P. C. C., Becker W., 2006, *ApJ*, **646**, 1104
- Burderi L., et al., 2001, *ApJ*, **560**, L71
- Burrows D. N., Hill J. E., Nousek J. A., Kennea J. A., Wells A., Osborne 2005, *Space Science Reviews*, **120**, 165
- Caraveo P. A., 2014, *ARA&A*, **52**, 211
- Cash W., 1979, *ApJ*, **228**, 939
- Chabrier G., Baraffe I., Allard F., Hauschildt P., 2000, *ApJ*, **542**, 464
- Chen K., 1991, *Nature*, **352**, 695
- Cheng Z., Li Z., Xu X., Li X., 2018, *ApJ*, **858**, 33
- Eggleton P. P., 1983, *ApJ*, **268**, 368
- Fabian A. C., Pringle J. E., Rees M. J., 1975, *MNRAS*, **172**, 15p
- Forbes D. A., Bridges T., 2010, *MNRAS*, **404**, 1203
- Forestell L. M., Heinke C. O., Cohn H. N., Lugger P. M., Sivakoff G. R., Bogdanov S., Cool A. M., Anderson J., 2014, *MNRAS*, **441**, 757
- Gehrels N., Chincarini G., Giommi P., Mason K. O., Nousek J. A., Wells A. A., White N. E., 2004, *ApJ*, **611**, 1005
- Geller A. M., et al., 2017, *ApJ*, **840**, 66
- Gentile P. A., et al., 2014, *ApJ*, **783**, 69
- Harding A. K., Usov V. V., Muslimov A. G., 2005, *ApJ*, **622**, 531
- Harris W. E., 1996, *AJ*, **112**, 1487
- Heinke C. O., 2010, in Kalogera V., van der Sluys M., eds, American Institute of Physics Conference Series Vol. 1314, American Institute of Physics Conference Series. pp 135–142 ([arXiv:1101.5356](https://arxiv.org/abs/1101.5356)), [doi:10.1063/1.3536355](https://doi.org/10.1063/1.3536355)
- Heinke C. O., Rybicki G. B., Narayan R., Grindlay J. E., 2006, *ApJ*, **644**, 1090
- Hertz P., Grindlay J. E., 1983, *ApJ*, **275**, 105
- Hills J. G., 1976, *MNRAS*, **175**, 1P
- Johnston H. M., Verbunt F., Hasinger G., 1994, *A&A*, **289**, 763
- King A. R., 1988, *QJRAS*, **29**, 1
- Linares M., 2014, *ApJ*, **795**, 72
- Lorimer D. R., Kramer M., 2004, *Handbook of Pulsar Astronomy*
- Lynch R. S., Ransom S. M., Freire P. C. C., Stairs I. H., 2011, *Astrophysical Journal*, **734**, 89
- Manchester R. N., Taylor J. H., 1977, *Pulsars*
- Nardiello D., et al., 2018, *MNRAS*, **481**, 3382
- Papitto A., et al., 2013, *Nature*, **501**, 517
- Pavlov G. G., Kargaltsev O., Garmire G. P., Wolszczan A., 2007, *ApJ*, **664**, 1072
- Piotto G., et al., 2015, *AJ*, **149**, 91
- Roberts M. S. E., McLaughlin M. A., Gentile P. A., Ray P. S., Ransom S. M., Hessels J. W. T., 2015, preprint, ([arXiv:1502.07208](https://arxiv.org/abs/1502.07208))
- Roberts M. S. E., et al., 2018, in Weltevrede P., Perera B. B. P., Preston L. L., Sanidas S., eds, IAU Symposium Vol. 337, Pulsar Astrophysics the Next Fifty Years. pp 43–46 ([arXiv:1801.09903](https://arxiv.org/abs/1801.09903)), [doi:10.1017/S1743921318000480](https://doi.org/10.1017/S1743921318000480)
- Romani R. W., Sanchez N., 2016, *ApJ*, **828**, 7
- Shishkovsky L., et al., 2018, *ApJ*, **855**, 55
- Simioni M., et al., 2018, *MNRAS*, **476**, 271
- Sirianni M., et al., 2005, *PASP*, **117**, 1049
- Stappers B. W., et al., 2014, *ApJ*, **790**, 39
- Strader J., et al., 2019, *ApJ*, **872**, 42
- Sutantyo W., 1975, *A&A*, **44**, 227
- The Fermi-LAT collaboration 2019, arXiv e-prints, p. [arXiv:1902.10045](https://arxiv.org/abs/1902.10045)
- Verner D. A., Ferland G. J., Korista K. T., Yakovlev D. G., 1996, *Astrophysical Journal*, **465**, 487
- Wadiasingh Z., Harding A. K., Venter C., Böttcher M., Baring M. G., 2017, *ApJ*, **839**, 80
- Webb N. A., Servillat M., 2013, *A&A*, **551**, A60
- Webb N. A., Gendre B., Barret D., 2002, *A&A*, **381**, 481
- Webb N. A., Serre D., Gendre B., Barret D., Lasota J.-P., Rizzi L., 2004, *A&A*, **424**, 133
- Wilms J., Allen A., McCray R., 2000, *Astrophysical Journal*, **542**, 914
- Zavlin V. E., 2007, *Ap&SS*, **308**, 297
- Zavlin V. E., Pavlov G. G., Shibanov Y. A., 1996, *A&A*, **315**, 141
- Zhou J. N., Zhang P. F., Huang X. Y., Li X., Liang Y. F., Fu L., Yan J. Z., Liu Q. Z., 2015, *MNRAS*, **448**, 3215
- de Martino D., et al., 2015, *MNRAS*, **454**, 2190